Int. J. Electrochem. Sci., 9 **(2014)** 1366 - 1377

International Journal of
ELECTROCHEMICAL
SCIENCE
www.electrochemsci.org

Electrochemical Determination of Carbaryl by Using a Molecularly Imprinted Polymer/Graphene-Ionic Liquid-Nano Au/chitosan-AuPt Alloy Nanoparticles Composite Film Modified Electrode

Lijuan Zhao, Faqiong Zhao, Baizhao Zeng[*]

Key Laboratory of Analytical Chemistry for Biology and Medicine (Ministry of Education), College of Chemistry and Molecular Sciences, Wuhan University, Wuhan 430072, Hubei Province, P. R. China
[*]E-mail: bzzeng@whu.edu.cn

Received: 13 November 2013 / *Accepted:* 9 December 2013 / *Published:* 5 January 2014

In this paper, a novel sensitive and selective molecularly imprinted electrochemical sensor was presented for the determination of carbaryl (1-naphthyl methylcarbamate). The sensor was constructed by coating a glassy carbon electrode (GCE) with chitosan-AuPt alloy nanoparticles (CS-AuPtNPs), graphene-ionic liquid-nano Au (GR-IL-Au), and followed by electrodepositing carbaryl imprinted poly(p-aminothiophenol) (p-ATP) film. The CS-AuPtNPs and GR-IL-Au composites played the roles to immobilize monomer p-ATP and to improve the electrochemical response; $[Fe(CN)_6]^{3-}/[Fe(CN)_6]^{4-}$ acted as electrochemical probe. The mechanism of the fabrication process and several important parameters controlling the preparation and electrochemical response of sensor were discussed and optimized. Under the optimal conditions, a linear range from 0.030 μM to 6.0 μM for the detection of carbaryl was obtained. The sensitivity was 4.0 μA/μM mm^2 and the detection limit was 8.0 nM (S/N=3). The resulting sensor displayed good selectivity and stability towards carbaryl. It was successfully applied to the determination of carbaryl in practical samples and the recovery was 96 − 105%.

Keywords: Carbaryl; Electrochemistry; Molecularly imprinted polymer; AuPt alloy nanoparticles; Graphene−ionic liquid−Au composites; p-Aminothiophenol

1. INTRODUCTION

Carbaryl, a major active ingredient of many commercial formulations of pesticide, is extensively used for pest control, such as plant hoppers, onion thrips and fruit flies [1, 2]. However, carbaryl residue in food, water and environment has severe threat to human health due to its high

toxicity to acetylcholinesterase (AChE), which is essential for the central nervous system of humans [3, 4]. Thus the sensitive detection of carbaryl residue is important. Up to now, many detection methods have been proposed for carbaryl, such as chromatography [5], spectrophotometry [6] and immunoassay [7]. These methods are sensitive and reliable, but they usually suffer from expensive instrumentation, cumbersome sample pretreatment and time-consuming [8]. Compared with them, electroanalytical method shows excellent sensitivity, rapid response and low cost, which have obtained wide applications in medical, biological and environmental analysis [9]. However, there are few reports on the electrochemical detection of carbaryl, probably due to its weak electrochemical activity. For example, Codognoto *et al.* [10] employed a boron doped diamond electrode to detect carbaryl, the linear range was 2.5 μM - 30.0 μM and the detection limit was 41 nM; Moraes *et al.* [11] prepared a multi-walled carbon nanotube/cobalt phthalocyanine modified electrode for carbaryl detection, the linear range was 0.33 μM - 6.6 μM and the detection limit was 5.46 nM. The electroanalytical methods were quite sensitive, but showed poor selectivity. Therefore, to fabricate new electrochemical sensors with high selectivity for carbaryl is necessary.

Molecularly imprinted polymers (MIPs) are biomimetic recognition materials that have advantages of high chemical stability, low cost and high selectivity [12, 13]. These properties make them very suitable for fabricating chemical/biological sensors with enhanced selectivity [14, 15]. For the construction of MIP-based sensors, molecularly imprinted films can be directly synthesized on electrode surface by electropolymerization, avoiding the problems of film unevenness or poor adhesion to the electrode, and the polymer thickness can be easily controlled by regulating the electrochemical conditions [16, 17]. For example, Pan *et al.* [18] reported a novel amperometric sensor based on metolcarb-imprinted film, which exhibited good binding affinity and selectivity for the template and could be used to accurately determine metolcarb in complex samples; Xie *et al.* [19] adopted a surface molecular self-assembly strategy and electropolymerization to prepare chlorpyrifos imprinting polymer sensor, which showed specific recognition selectivity for chlorpyrifos molecules over other pesticides and exhibited high stability. Although MIP can improve selectivity, it generally makes sensitivity decrease. In order to achieve high sensitivity, many new functional materials are employed to construct the substrate layer for MIP, such as conducting polymer [20], graphene (GR) [21] and metallic nanomaterials [22].

Metallic nanomaterials, especially nobel metal nanomaterials and alloy nanomaterials, have high conductivity and catalytic activity etc. Hence they are widely used in fabricating electrochemical sensors [23] and biosensors [24]. In addition, some metals can combine molecules with -CN, $-NH_3$ or -SH groups [25], hence they can also immobilize functional molecules or monomers.

As for graphene (GR), which has advantages of excellent electrical conductivity, high chemical stability and large surface [26, 27], is quite promising as a electrode material. Recently, the functionalization of graphene with metal nanomaterials received increasing attention [28, 29], and GR is proved to be a good support material for loading them. Thus GR and metal nanomaterials can be combined in preparing electrochemical sensors.

In this work, graphene-ionic liquid-nano Au hybrid (GR-IL-Au) was synthesized by chemical co-reduction of graphene oxide (GO) and $HAuCl_4$ in the presence of ionic liquid, and a chitosan-AuPt alloy nanoparticles (CS-AuPtNPs)/GR-IL-Au composite modified GCE was prepared, then carbaryl

imprinted poly(p-aminothiophenol) was electrodeposited on the composite film for the detection of carbaryl, using $[Fe(CN)_6]^{3-}$/$[Fe(CN)_6]^{4-}$ as electrochemical probe. Owing to the synergistic effect of several components in the composite, the modified electrode showed high selectivity, stability and sensitivity to detect carbaryl. In addition, the sensors were successfully applied to the determination of carbaryl in practical samples.

2. EXPERIMENTAL

2.1 Reagents and materials

Carbaryl, metolcarb, isoprocarb, fenobucarb and propoxur were purchased from Aladdin Chemistry Co., Ltd. (Shanghai, China), and their stock solutions (0.010 M) were prepared with ethanol and stored in a refrigerator. p-Aminothiophenol (p-ATP) and tetrabutylammonium perchlorate (≥ 99%) were obtained from Sigma-Aldrich (Madrid, Spain). Chitosan (CS) was purchased from Regal Biotechnology Co., Ltd. (Shanghai, China). $HAuCl_4$ and H_2PtCl_6 were from Sinopharm Chemical Reagent Co. Ltd. (Shanghai, China). The ionic liquid 1-(2'-hydroxylethyl)-3-methylimidazolium bis[(trifluoromethyl)sulfonyl]imide ([HeMIM][NTf_2]) (purity: 99%) was provided by Lanzhou Institute of Chemical Physics (Lanzhou, China) and used as received. Graphene oxide came from Xianfeng Reagent Co. Ltd. (Nanjing, China). Hydrazine hydrate (85%) was obtained from Sinopharm Chemical Reagent Co., Ltd. (Shanghai, China). All other chemicals used were of analytical reagent grade. The water used was redistilled.

2.2 Apparatus

Cyclic voltammetric and differential pulse voltammetric experiments were performed with a CHI 620D electrochemical workstation (CH Instrument Company, Shanghai, China). A conventional three-electrode system was adopted. The working electrode was a modified glassy carbon electrode (GCE, diameter: 2 mm), and the auxiliary and reference electrodes were a Pt wire and a saturated calomel electrode (SCE), respectively. Scanning electron microscope (SEM) images were obtained using field emission SEM (ZEISS, Germany). Transmission electron microscopy (TEM) images were obtained using a JEM-2100 microscope (JEOL Ltd., Japan). All experiments were carried out at room temperature.

2.3 Preparation of CS-AuPtNPs

CS-AuPtNPs was synthesized according to literature with minor modification [30]. Firstly, a 0.1 % CS stock solution was prepared by dissolving 100 mg CS into 100 mL 1.0 % (V/V) acetic acid solution. Then 68.7 μL $HAuCl_4$ and 172.7 μL H_2PtCl_6 aqueous solutions (both 10 mg/mL) were added to 4.12 mL above CS solution. At last, 614 μL $NaBH_4$ aqueous solution (10 mM) was added to the resulting mixture. The solution was stirred for 5 h at room temperature. Therefore, CS-AuPtNPs

composite was obtained. The AuPtNPs were proved to be alloy [30], and the atomic ratio of Pt/Au was about 2:1.

2.4 Preparation of GR-IL-Au

A 10 mg GO was dispersed into 10 mL water, followed by addition of 35 mg NaOH and 40 μL [HeMIM][NTf_2]. After ultrasonication for 30 min, 418 μL $HAuCl_4$ aqueous solution (10mg/mL) was added and the mixture was stirred for 12 h at 80 °C. Afterwards, 6 mL hydrazine (85%) was introduced under stirring and the solution was kept at 80 °C for 24 h. After the reaction was completed, the product was centrifuged, washed with water and ethanol for three times, and then it was dissolved into 10 mL water. For comparison, GR-Au composite was prepared by a similar way.

2.5 Preparation of MIP/GR-IL-Au/CS-AuPtNPs/GCE

The molecularly imprinted modified electrode was prepared according to the following produce. First of all, 6 μL CS-AuPtNPs was dropped on the surface of a cleaned GCE; after the solvent was evaporated in air, 4 μL GR-IL-Au was transferred on the CS-AuPtNPs modified electrode and let it dry in air. Secondly, the obtained GR-IL-Au/CS-AuPtNPs/GCE was immersed into 30 mM p-ATP (in ethanol) for 18 h to allow monomer to self-assemble, and then washed thoroughly with ethanol. After that, the p-ATP modified GR-IL-Au/CS-AuPtNPs/GCE was immersed into 10 mM carbaryl (in ethanol) for 6 h. The electrode was taken out, rinsed with ethanol and dried under nitrogen flow.

Finally, the electropolymerization was performed in an ethanol solution containing 2.5 mM carbaryl, 5 mM tetrabutylammonium perchlorate and 12.5 mM p-ATP. The cyclic potential range was -0.2 V − 1.4 V; scan rate was 50 mV s^{-1}; potential scan was repeated for 10 times. After electropolymerization, the composite film modified electrode was rinsed with 20% ethanol − 0.2 M HCl solution for three times (each for 5 min) to remove the template molecules. Therefore, a MIP/GR-IL-Au/CS-AuPtNPs/GCE was obtained. At the same time, a MIP/GR-IL-Au/GCE was produced under identical conditions. For comparison, a NIP/GR-IL-Au/CS-AuPtNPs/GCE was prepared and treated by the same way.

2.6 Electrochemical measurements

The MIP/GR-IL-Au/CS-AuPtNPs/GCE was dipped into desired carbaryl solution (in ethanol) for 18 min, and then it was transferred to the electrochemical cell containing 5 mM $[Fe(CN)_6]^{3-}/[Fe(CN)_6]^{4-}$ and 0.2 M KCl for electrochemical measurements. The cyclic voltammograms (CV) and differential pulse voltammograms (DPV) were recorded between -0.2 V and +0.6 V. The change of peak current (ΔI) was used for quantification. After every measurement, the electrode was rinsed with 20% ethanol − 0.2 M HCl to remove carbaryl for reuse. All experiments were performed at room temperature.

3. RESULTS AND DISCUSSION

3.1 Characterization of CS-AuPtNPs and GR-IL-Au composites

The morphological aspect of CS-AuPtNPs is shown in Fig. 1a, the AuPtNPs homogeneously distribute on the surface of CS, with an average particle diameter of about 5 nm. In this case, CS virtually acts as a stabilizer and support [31]. As shown in Fig. 1b, GR displays flake-like shape and nano Au is spherical, which has an average diameter of about 30 nm. The nano Au loaded on GR shows low density and poor dispersion. However, under the influence of IL, the nano Au loaded on GR is more uniform and dense (Fig. 1c). Furthermore, the shape of nano Au is anisotropic, indicating that IL plays an important role in the formation of nano Au. Part of this can be ascribed to the template function of IL [32].

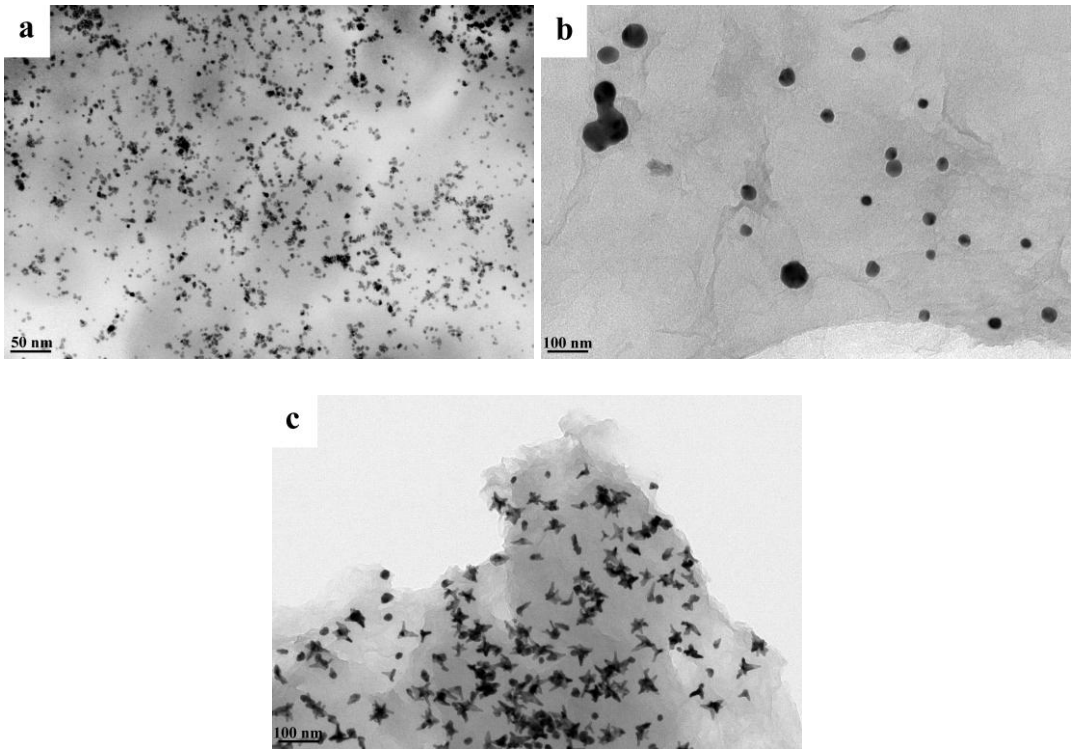

Figure 1. TEM of CS-AuPtNPs composite (A), GR-Au composite (B) and GR-IL-Au composite (C).

3.2 Fabrication of modified electrode

CS-AuPtNPs and GR-IL-Au are modified on a GCE as the first and second layer, respectively. As CS is an immobilization matrix for the construction of sensors [33], the CS-AuPtNPs is well immobilized on the surface of GCE. The GR-IL-Au composite contains IL, which is favorable for the immobilization of GR-IL-Au due to its adhesive effect. Furthermore, the -OH group of IL can also form hydrogen bond with CS-AuPtNPs layer. When the GR-IL-Au/CS-AuPtNPs/GCE is immersed into p-ATP solution, p-ATP molecules self-assemble on the GR-IL-Au composite surface by forming Au-S bonds. On the other hand, when the p-ATP modified GR-IL-Au/CS-AuPtNPs/GCE is immersed

into carbaryl solution, the carbaryl molecules assemble on the electrode surface through forming hydrogen bond between the residual amino group of p-ATP and nitrogen/oxygen atom of carbaryl. After the electropolymerization of p-ATP, these carbaryl molecules are embedded into the poly(p-ATP) film and form imprinted sites. The SEM image of MIP/GR-IL-Au/CS-AuPtNPs film presents rough surface, indicating it can provide a large surface area for the adsorption of target molecules [19].

3.3 Electrochemical behavior of the modified electrodes

Fig. 2a shows the CVs of CS-AuPtNPs/GCE, GR-IL-Au/CS-AuPtNPs/GCE and MIP/GR-IL-Au/CS-AuPtNPs/GCE in $[Fe(CN)_6]^{3-}/[Fe(CN)_6]^{4-}$ solution. A couple of well-defined redox peaks appear at bare GCE which is characteristic of reversible electron transfer process of redox $[Fe(CN)_6]^{3-}/[Fe(CN)_6]^{4-}$ (curve A). As shown in Curve B, when GCE surface is covered with CS-AuPtNPs, the peak currents increase greatly due to the increase of effective electrode area. Furthermore, with the addition of GR-IL-Au on the CS-AuPtNPs modified electrode, the GR-IL-Au/CS-AuPtNPs/GCE exhibits much higher peak currents, indicating that it has much bigger surface area (curve C). Curve D shows the CV of the senor after electropolymerization of p-ATP film in the presence of carbaryl, the peak currents declined obviously, indicating that the MIP retards the electron transfer due to its poor conductivity. As shown in Curve E, the peak currents of the electrode increased apparently after the template was removed. The reason is that vacant recognition sites occur, which permit the probe molecules to reach the conductive surface. Fig. 2b shows the CVs of GR-IL-Au/GCE and MIP/GR-IL-Au/GCE, their peak currents are smaller in comparison with those of GR-IL-Au/CS-AuPtNPs/GCE and MIP/GR-IL-Au/CS-AuPtNPs/GCE, respectively. Especially, the MIP/GR-IL-Au/CS-AuPtNPs/GCE exhibits larger peak current change for removing template molecules or not, meaning that it has more available recognition sites than MIP/GR-IL-Au/GCE. Therefore, MIP/GR-IL-Au/CS-AuPtNPs/GCE was adopted in this work.

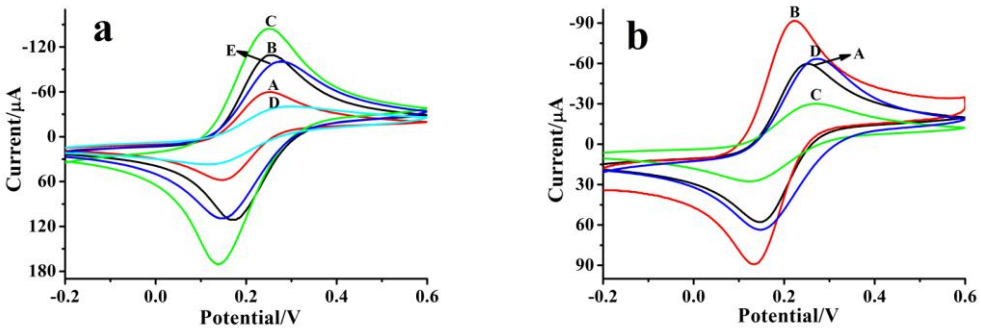

Figure 2. (a) CVs of bare GCE (A), CS-AuPtNPs/GCE (B), GR-IL-Au/CS-AuPtNPs/GCE (C), MIP/GR-IL-Au/CS-AuPtNPs/GCE before removing template (D), MIP/GR-IL-Au/CS-AuPtNPs/GCE after removing template (E). (b) CVs of bare GCE (A), GR-IL-Au/GCE (B), MIP/GR-IL-Au/GCE before removing template (C), MIP/GR-IL-Au/GCE after removing template (D). Scan range: -0.2 V to +0.6 V; scan rate: 100 mV s^{-1}; solution composition: 5 mM $[Fe(CN)_6]^{3-}/[Fe(CN)_6]^{4-}$ + 0.2 M KCl.

3.4 Optimization of parameters affecting the determination of carbaryl

3.4.1 Influence of the concentration ratio of H_2PtCl_6 to $HAuCl_4$ and the amount of CS-AuPtNPs

As shown in Fig. 3a, the Δ*I* increases with decreasing ratio of $c(H_2PtCl_6)/c(HAuCl_4)$, and reaches a maximum value at 2:1. Then it decreases with further decreasing the proportion of H_2PtCl_6. Therefore, the concentration ratio of 2:1 (H_2PtCl_6 to $HAuCl_4$) was selected.

The amount of CS-AuPtNPs was also varied to examine its influence (Fig. 3b). As a result, with increasing the amount of CS-AuPtNPs, the Δ*I* increases. When it is 6 μL, maximum current response is obtained. The reason is that the effective electrode area is related to the amount of CS-AuPtNPs. But when it exceeds 6 μL, the film becomes thick, which hinders the electron-transfer and makes Δ*I* decrease.

3.4.2 Optimization of IL concentration and the amount of GR-IL-Au

Considering the key role of IL, the concentration of IL was changed in preparing GR-IL-Au composite to explore its influence. As shown in Fig. 3c, Δ*I* increases rapidly when IL concentration is changed from 1 μL/mL to 4 μL/mL, and then it decreases. This can also be ascribed to the effect of IL on the effective electrode area, as IL influences the density and dispensability of nano Au. As a result, 4 μL/mL was chosen in this work.

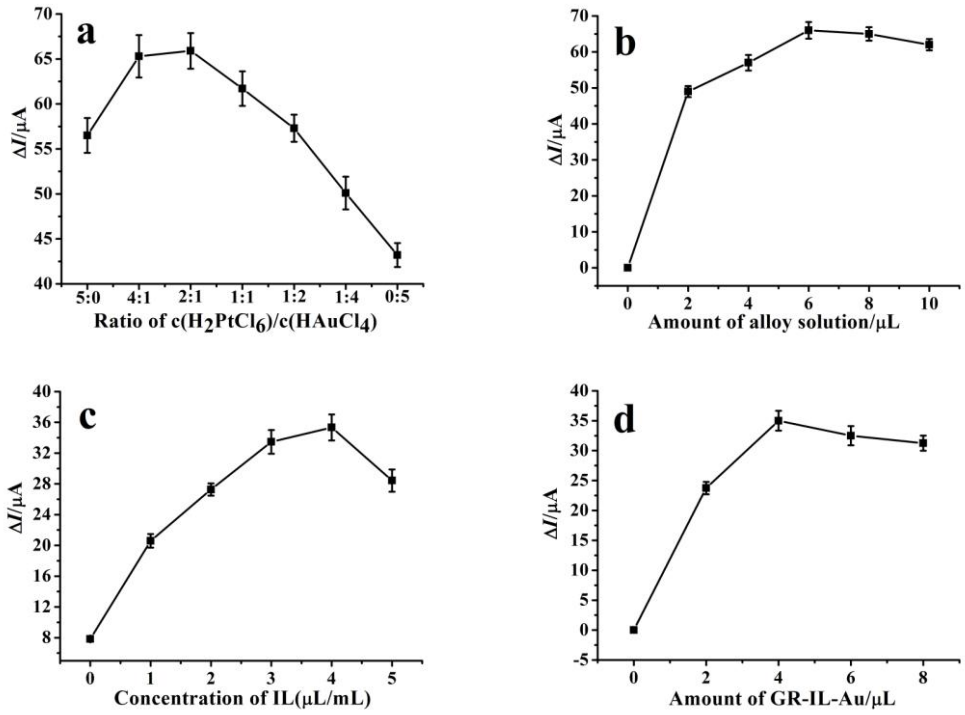

Figure 3. Effect of the concentration ratio of H_2PtCl_6 to $HAuCl_4$ (a); the amount of CS-AuPtNPs solution (b); Effect of IL concentration (c) and the amount of GR-IL-Au suspension (d). Solution composition for determination: 5 mM $[Fe(CN)_6]^{3-}/[Fe(CN)_6]^{4-}$ + 0.2 M KCl; The pulse amplitude, potential increment, pulse width and pulse period in DPV were set up at 50 mV, 5 mV, 100 ms and 200 ms, respectively.

The influence of the amount of GR-IL-Au was also studied. Results show that Δ*I* increases with the volume of GR-IL-Au suspension going up to 4 μL (Fig. 3d), then it decreases slowly. The reason is similar to that of CS-AuPtNPs. In this case, 4 μL of GR-IL-Au suspension was adopted.

3.4.3 Optimization of the mole ratio of template molecule to functional monomer, the electropolymerization time and the adsorption time

The mole ratio of template to functional monomer is a very important factor in the preparation of imprinted film. As shown in Fig. 4a, the biggest Δ*I* value is obtained when the mole ratio is 1:5. When it is lower or higher than 1:5, the current response decreases. This is related to the change of binding-site number. When the functional monomer is relatively less, a small number of available binding sites are produced as there are not enough monomer molecules to interact with template molecules. On the other hand, when functional monomer is relatively more, there are not enough template molecules for binding, thus the quantity of available binding sites is less. In this case, the mole ratio of 1:5 should be the balance point. Besides, the electropolymerization time is also important. When it is shorter (e.g. cycling potential for 5 or 8 times), the MIP film is very thin and unstable. When it is too long (e.g. cycling potential for more than 15 times), the current response is small due to the formation of a thick MIP film, which has high mass-transfer resistance. At the same time, the template molecules cannot be completely removed. Here, electropolymerization was performed by cycling the potential for 10 times.

In addition, to examine the influence of incubation time on the current response of the sensor, the imprinted sensor was incubated in 1 μM carbaryl solution for different time. As shown in Fig.4b, the current response Δ*I* increases with increasing incubation time. But when it exceeds 18 min, Δ*I* keeps almost unchanged, indicating that the adsorption equilibrium is reached. Herein, 18 min was selected.

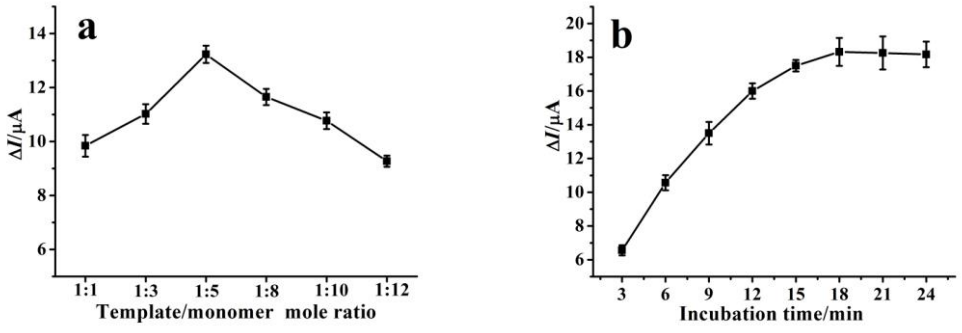

Figure 4. Effect of mole ratio of template to monomer (a) and incubation time (b) on the response current of 1μM carbaryl. Other conditions as in Fig. 3.

3.5 Calibration curves

Fig. 5 displays the DPVs of MIP/GR-IL-Au/CS-AuPtNPs/GCE under the optimized experimental conditions. As can be seen, the peak current decreases with carbaryl concentration

increasing. A linear relationship between the Δ*I* value and carbaryl concentration is obtained in the concentration range from 0.030 μM to 6.0 μM (The inset of Fig. 5). The linear regression equation is Δ*I* (μA) = 12.6 c (μM) + 5.4 (R^2=0.997), with a sensitivity of 4.0 μA/μM mm^2. The limit of detection is 8.0 nM (S/N=3). When the concentration of carbaryl is higher than 6.0 μM, the current response tends to be stable, indicating that the imprinted cavities are almost occupied by carbaryl molecules. In comparison with the doped diamond electrode and multi-walled carbon nanotubes/cobalt phthalocyanine modified electrode, the MIP/GR-IL-Au/CS-AuPtNPs/GCE presents better performance [10, 11].

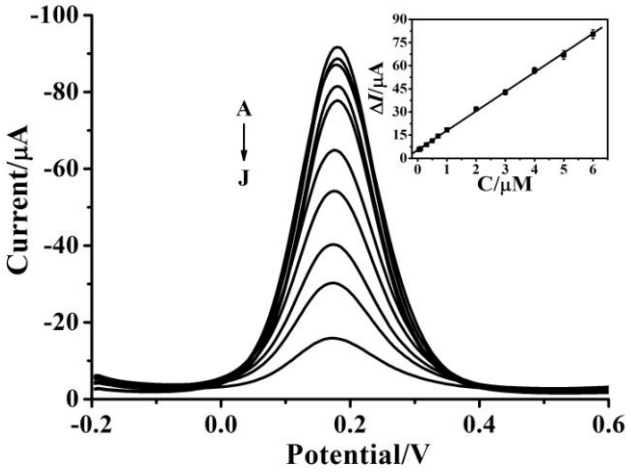

Figure 5. DPVs of MIP/GR-IL-Au/CS-AuPtNPs/GCE after incubating in carbaryl solution. Carbaryl concentration (from A to J): 0, 0.30, 0.50, 0.70, 1.0, 2.0, 3.0, 4.0, 5.0, 6.0 μM. The inset shows the calibration curves of carbaryl at MIP/GR-IL-Au/CS-AuPtNPs/GCE. Other conditions as in Fig. 3.

3.6 Selectivity, repeatability and stability of MIP/GR-IL-Au/CS-AuPtNPs/GCE

The selectivity of the MIP/GR-IL-Au/CS-AuPtNPs/GCE was evaluated by testing the Δ*I* value caused by carbaryl and other analogues and potential interfering substances, such as metolcarb, isoprocarb, fenobucarb and propoxur. As shown in Fig. 6, compared with the NIP sensor, the Δ*I* of the imprinted sensor is larger than that of the non-imprinted sensor, which is approximately 4.58 times larger than NIP/GR-IL-Au/CS-AuPtNPs/GCE, and the Δ*I* caused by carbaryl is much larger than that by structural analogs. This might attribute that the size and array of the functional group of cavities matching with the template molecular carbaryl in the MIP film, so the diffusion of carbaryl to the surface of electrode is much easier than that of other interfering species. This confirmed that the MIP/GR-IL-Au/CS-AuPtNPs/GCE had good selectivity.

The reproducibility of the imprinted sensor was evaluated by determining 1 μM carbaryl solution under the same conditions using three electrodes prepared with different batches of MIPs and the relative standard deviation (RSD) of the response current was 5.3% (n = 3). For the consecutive determination of a 1 μM carbaryl solution using one modified electrode, the RSD of response current

was 4.7% (n = 5). This reflects the good reproducibility of the proposed method. Furthermore, the electrode retains about 91.2% of the initial response current after storing for two week. This indicates that the MIP/GR-IL-Au/CS-AuPtNPs/GCE has good stability.

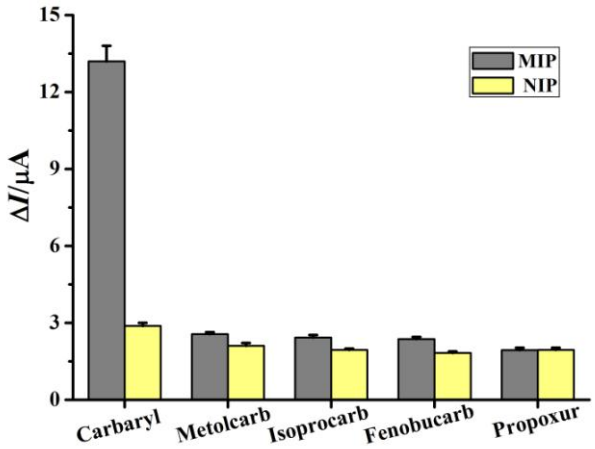

Figure 6. Current response of the imprinted and non-imprinted sensors towards 1 μM carbaryl, metolcarb, isoprocarb, fenobucarb and propoxur. Other conditions as in Fig. 3.

3.7 Analytical application of MIP/GR-IL-Au/CS-AuPtNPs/GCE

In order to test its application feasibility, the method was applied to the detection of carbaryl in practical samples such as cabbage and apple peel. Prior to determination, they were grinded to slurry and centrifuged, then 1.0 mL of the supernatant was weighed and diluted to 10 mL with ethanol for determination. But no carbaryl was detected in these samples. Standard carbaryl solutions were added to the sample solutions and the recovery was estimated. The results were summarized in Table 1 and the recovery was 96 − 105% for different samples and different concentration levels. This suggests that the proposed method is reliable.

Table 1. Determination results of carbaryl in samples using a MIP/GR-IL-Au/CS-AuPtNPs/GCE (n = 3).

Samples	Carbaryl added (μM)	Carbaryl found (μM)	Recovery (%)
Cabbage	0	-	-
	0.5	0.49±0.06	98
	1.0	0.96±0.09	96
	5.0	5.2±0.3	104
Apple peel	0	-	-
	0.5	0.51±0.05	102
	1.0	1.05±0.04	105
	5.0	4.8±0.2	96

4. CONCLUSIONS

A novel molecularly imprinted polymer/grapheme-ionic liquid-nano Au/chitosan-AuPt alloy nanoparticles composite film coated glassy carbon electrode (MIP/GR-IL-Au/CS-AuPtNPs/GCE) is fabricated for carbaryl sensing. The modified electrode has large specific surface and more binding sites, and exhibits high selectivity, reproducibility and sensitivity. The electrode can be applied to the determination of carbaryl in real samples. This novel and facile strategy can be further used to fabricate other electrochemical sensors.

ACKNOWLEDGEMENTS
The authors appreciate the financial support of the National Natural Science Foundation of China (Grant Nos.: 21075092, 21277105).

References

1. V.A. Pedrosa, J. Caetano, S.A.S. Machado and M. Bertotti, *Sensors*, 8 (2008) 4600
2. T.N. Rao, B.V. Sarada, C. Terashima and A. Fujishima, *Anal. Chem.*, 74 (2002) 1578
3. A. Santalad, L. Zhou, F. Shang, D. Fitzpatrick, R. Burakham, S. Srijaranai, J.D. Glennon and J.H. Luong, *J. Chromatogr. A*, 1217 (2010) 5288
4. X.J. Wang, L. Chen, S.Q. Xia, Z.L. Zhu, J.F. Zhao, J.M. Chovelon and N.J. Renaul, *Int. J. Electrochem. Sci.*, 1 (2006) 55
5. S.S. Petropoulou, A. Tsarbopoulos and P.A. Siskos, *Anal. Bioanal. Chem.*, 385 (2006) 1444
6. N.L. Pacioni and A.V. Veglia, *Anal. Chim. Acta*, 488 (2003) 193
7. D. Du, W. Chen, J. Cai, J. Zhang, F. Qu and H. Li, *J. Electroanal. Chem.*, 623 (2008) 81
8. J. Cancino, C.A. Razzino, V. Zucolotto and S.A.S. Machado, *Electrochim. Acta*, 87 (2013) 717
9. C. Wang, C. Li, F. Wang and C. Wang, *Appl. Surf. Sci.*, 253 (2006) 2282
10. L. Codognoto, S.T. Tanimoto, V.A. Pedrosa, H.B. Suffredini, S.A.S. Machado and L.A. Avaca, *Electroanal.*, 18 (2006) 253
11. F.C. Moraes, L.H. Mascaro, S.A.S. Machado and C.M.A. Brett, *Talanta*, 79 (2009) 1406
12. B. Rezaei, O. Rahmanian, *Sens. Actuators, B*, 160 (2011) 99
13. V. Suryanarayanan, C.T. Wu and K.C. Ho, *Electroanal.*, 22 (2010) 1795
14. T. Alizadeh, *Thin Solid Films*, 518 (2010) 6099
15. D. Zhang, D. Yu, W. Zhao, Q. Yang, H. Kajiura, Y. Li, T. Zhou and G. Shi, *Analyst*, 137 (2012) 2629
16. W. Lian, S. Liu, J. Yu , J. Li, M. Cui, W. Xu and J. Huang, *Biosens. Bioelectron.*, 44 (2013) 70
17. X. Liu, C. Li, C. Wang, T. Li and S. Hu, *J. Appl. Polym. Sci.*, 101 (2006) 2222
18. M.F. Pan, G.Z. Fang, B. Liu, K. Qian and S. Wang, *Anal. Chim. Acta*, 690 (2011) 175
19. C. Xie, H. Li, S. Li, J. Wu and Z. Zhang, *Anal. Chem.*, 82 (2009) 241
20. X. Zheng, X. Zhou, X. Ji, R. Lin and W. Lin, *Sens. Actuators, B*, 178 (2013) 359
21. X. Wang, J. Dong, H. Ming and S. Ai, *Analyst*, 138 (2013) 1219
22. S. Ge, M. Yan, J. Lu, M. Zhang, F. Yu, J. Yu, X. Song and S. Yu, *Biosens. Bioelectron.*, 31 (2012) 49
23. L. Bai, R. Yuan, Y. Chai, Y. Yuan, L. Mao, Y. Wang, *Anal. Chim. Acta*, 698 (2011) 14
24. B. Singh, F. Laffir, T. McCormac and E. Dempsey, *Sens. Actuators, B*, 150 (2010) 80
25. Y. Du, X.L. Luo, J.J. Xu and H.Y. Chen, *Bioelectrochem.*, 70 (2007) 342
26. M. Acik, D.R. Dreyer, C.W. Bielawski and Y.J. Chabal, *J. Phys. Chem. C*, 116 (2012) 7867
27. C. Ruan, T. Li, Q. Niu , M. Lu, J. Lou, W. Gao, W. Sun, *Electrochim. Acta*, 64 (2012) 183

28. F. Han, X. Wang, J. Lian and Y. Wang, *Carbon*, 50 (2012) 5498
29. S. Wang, X. Wang and S.P. Jiang, *Phys. Chem. Chem. Phys.*, 13 (2011) 6883
30. G. Yang, R. Yuan and Y.Q. Chai, *Colloids Surf., B*, 61 (2008) 93
31. H. Huang and X. Yang, *Biomacromolecules*, 5 (2004) 2340
32. Z. Li, A. Friedrich and A. Taubert, *J. Mater. Chem.*, 18 (2008) 1008
33. J. Peng, C. Hou and X. Hu, *Sens. Actuators, B*, 169 (2012) 81